Influence of the microchannel plate and anode gap parameters on the spatial resolution of an image intensifier

T. H. Hoenderken, C. W. Hagen,[a] J. E. Barth, and P. Kruit
Department of Applied Physics, Delft University of Technology, Lorentzweg 1, 2628 CJ Delft, The Netherlands

G. O. Nützel
Delft Electronic Products (DEP), Dwazziewegen 2, 9300 AB Roden, The Netherlands

(Received 19 September 2000; accepted 19 February 2001)

The spatial resolution that can be obtained with image intensifiers depends largely on the spatial resolution of the microchannel plate (MCP)-anode assembly. Existing models on MCPs never include the nonuniform anode field penetration into the channels. The objective of this article is to show that this field penetration leads to a lens effect which has a crucial influence on the electron trajectories and the spatial resolution that can be obtained. From a simple model the relevant parameters determining the spatial resolution are identified as the anode gap, the anode field, the end-spoiling penetration depth, and the channel diameter. These parameters are varied in a Monte-Carlo simulation in which 20 000 electrons are traced through a channel, the end-spoiling, and the anode gap. The spatial resolution as obtained from these simulations is shown to depend heavily on the nonuniform field at the end spoiling. Especially low-energy electrons generated at the end spoiling deteriorate the spatial resolution. The best resolution is obtained for a small anode gap (300 μm) and small anode voltage (3 kV). This indicates that, above a certain value of the electric field in the anode gap, the effect of the lens is dominant. Doubling the end-spoiling penetration depth from 10 to 20 μm increases the resolution especially at high spatial frequencies. Furthermore, the resolution is enhanced considerably by decreasing the channel diameter. These results can be fully understood from the simple model presented. In addition, results are presented from experiments in which the spatial resolution is measured for various anode gaps and anode voltages. The dependencies of the spatial resolution on these parameters are in good qualitative agreement with the simulation results. [DOI: 10.1116/1.1364701]

I. INTRODUCTION

Second generation proximity focused image intensifiers consist basically of a photocathode, a microchannel plate (MCP), and a phosphor screen. The photocathode converts the incoming photon image into electrons. This electron image is accelerated towards the MCP in the cathode gap. The major part of the electrons will arrive in a channel and impinge on the cylindrical surface, thereby generating secondary electrons. These are accelerated down the channel, now liberating electrons themselves. In this way a single incoming electron can lead to a cloud of, typically, 10^4 electrons leaving the MCP. This cloud will then be accelerated in the anode gap to gain the amount of energy that is necessary to light the phosphor grains, which display the electron image. In this type of image intensifier the proximity focusing is achieved by the application of homogeneous axial electrostatic fields in the cathode gap as well as in the anode gap.

This article deals with the spatial resolution of proximity focused MCP image tubes. In state-of-the-art image intensifiers one of the key factors that sets the resolution limit is the MCP-to-anode region of electron transfer.[1] To understand why, insight has to be gained in the way electrons move through the channels and the anode gap. In other words, the influence of the geometrical and electrical parameters on the electron trajectories needs to be understood.

A MCP consists of parallel arrays of hollow glass cylinders, which essentially are thin secondary emission current amplifiers. With a sufficiently high voltage over the MCP, collisions of energetic particles with the channel wall will lead to the emission of secondary electrons. Both sides of the MCP are covered with a thin layer of electrically conducting material, which is done first to connect all channels in parallel and second to provide the channels with a simple ''aperture'' at the output electrode (usually called the ''end spoiling'').

Koshida *et al.*[2,3] extensively discussed the energy distribution of the electrons that come out of the channels. They divided all electrons that come out of the channel into two major groups, which are:

Group (A): electrons that emerged from the end-spoiling region, which have a very low amount of kinetic energy V (typically 0 to 10 eV) at the moment they leave the channel, and

Group (B): electrons that emerged from the channel region before the end-spoiling region, for which the electron energy V is typically between 10 and 100 eV.

The energy distribution is the sum of the contributions

[a]Electronic mail: hagen@cpo.tn.tudelft.nl

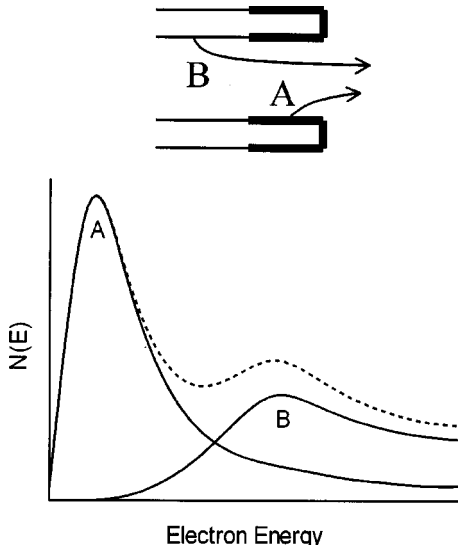

FIG. 1. Schematic drawing of the end of a channel with two typical electron trajectories (groups A and B) (top) and the corresponding energy distributions (bottom). The dashed line represents the total distribution.

from each group: a sharp low energy main peak (A) and a subpeak with a long tail (B), as shown in Fig. 1. As the end spoiling is almost field free the kinetic energy of an outcoming electron that is emitted from the end spoiling (group A) is almost equal to its emission energy. Now Koshida *et al.* state that electrons emitted from the end spoiling are preferable for a high spatial resolution. They argue that low energy electrons cannot travel far from the channel where they are emitted and thus cannot be responsible for the degradation in spatial resolution. However, the end-spoiling material usually has a relatively low secondary electron emission yield. Therefore, to enhance the spatial resolution, and to increase the gain as well, Koshida *et al.* proposed to deposit a more efficient secondary electron emission material onto the end-spoiling region. Unfortunately, there are no experiments or simulations to confirm these ideas.

In this article a full Monte-Carlo simulation of the electron trajectories inside the channels and between the end spoiling and the anode is described. From a simple model, the relevant parameters of secondary electrons and their trajectories are identified, and for various values of these parameters the simulations are performed. The resulting distribution of the electrons on the anode is a measure of the spatial resolution that can be obtained. Then experiments will be described to measure the spatial resolution for different anode gaps and anode voltages, and the results are compared to the simulation results. Finally, the results will be discussed and conclusions will be drawn.

II. SIMULATION MODEL

First the geometry, in which the electrons will be released, has to be defined. The elementary configuration is shown in Fig. 2. Typical values that are used in state-of-the-art image intensifiers are: anode gap $a=500$ μm, end-spoiling depth $h=20$ μm, channel diameter $d=10$ μm, and

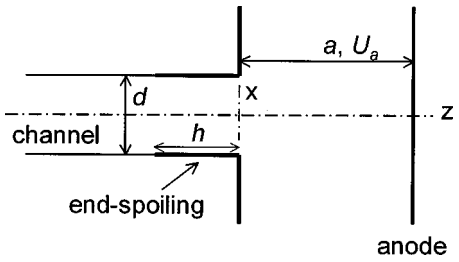

FIG. 2. The geometry that forms the basis of the simulation model. The default values are $a=500$ μm, $h=20$ μm, $d=10$ μm, and $U_a=5$ kV. The coordinate system is also shown.

anode gap voltage $U_a=5$ kV. A configuration with these values will be referred to as the default configuration. The positive z axis is directed from the channel towards the anode, and the origin is chosen to be at the channel end. Once the geometry is known, the electrostatic field can be calculated. This is done with the finite element method, using the electrostatic lens design program ELD.[4] The density of the mesh lines may vary, which offers the possibility to increase the accuracy of the calculated potential locally. This is done at the edges of the end spoiling where a considerable field enhancement is expected. Of course, the electric field is uniform in the anode gap and in the channel region before the end spoiling. However, it penetrates from both sides into the end-spoiling region, thereby creating a ''lens effect,'' as is shown in Fig. 3 for the anode gap side of the end spoiling. The lens effect has never been investigated in relation with the spatial resolution of image intensifiers.

Now before doing the full simulation it is instructive to estimate the importance of the lens effect using a very simplified model. As the anode field is typically about six times larger than the channel field in image intensifiers, the lens effect is only expected to have a serious influence on the anode gap side of the end spoiling. An estimate (thin lens approximation) of the focal length F of the lens is given by[5]

$$F=\frac{4V_z}{E_a}, \tag{1}$$

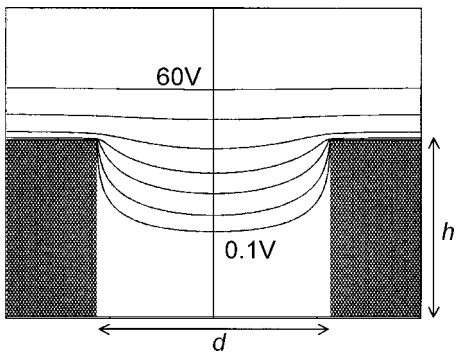

FIG. 3. Detailed view of the end-spoiling edge for the earlier mentioned default values. The end-spoiling potential is 0 V; the equipotential lines shown are 0.1, 0.3, 1.0, 3.0, 10, 30, and 60 V (from bottom to top resp.). The enhancement of the field is considerable, especially near the end-spoiling edges.

where V_z is the axial electron energy (eV) at the lens and E_a is the electric field in the anode gap. Two things can happen to an electron that is emitted from the channel wall: (i) it collides with the channel wall again (thereby generating secondaries) or (ii) it escapes from the channel and reaches the anode. Of course, this is fully dependent on the exit angle and energy of the secondary electron. Once the electron has entered the homogeneous field between MCP and anode, the trajectory is a simple parabola. One can write for the distance between the point of arrival on the anode of an outcoming electron and the point where the channel axis intersects the anode

$$R_a \approx 2a\left(\frac{V_\perp}{U_a}\right)^{1/2}, \tag{2}$$

where $V_\perp$ is the radial energy of the electron, a is the anode gap, and U_a is the voltage over the anode gap. Consequently, one would expect that a higher anode voltage is preferable for a smaller electron spot on the anode. For example, if $V_\perp = 2$ eV then R_a becomes 20 μm (for the default values from Fig. 2).

However, the lens at the end of the end spoiling will change the radial velocity $\nu_\perp$ of the electrons which come from far behind the lens (group B electrons) with an amount $\nu_z \tan(\xi)$, where ν_z is the axial velocity and ξ is the angle between ν_z and the total velocity ν after the electron has passed the lens. Thus $V_\perp$ consists of two components, i.e.,

$$V_\perp = V_{\perp,0}(\text{radial emission energy}) + V_{\perp,\text{lens}}(\text{radial energy change due to lens}). \tag{3}$$

To estimate the effect of the radial energy change one can write $\tan(\xi) = rF^{-1}$ where r is the distance from the optical axis to the electron just before it crosses the lens. With this and Eq. (1), the point of arrival on the anode, due to the radial momentum change only, becomes

$$(\text{group B})\ R_a \approx \frac{r}{2}\left(\frac{U_a}{V_z}\right)^{1/2}. \tag{4}$$

Note that this is independent of the anode gap. With $V_z = 50$ eV and $r = 4$ μm, this leads to an R_a of 20 μm (for the default values). With two contributions to R_a, of which one is proportional to $\sqrt{U_a}$ and one is proportional to $1/\sqrt{U_a}$, there must be an optimum U_a. At the optimum U_a both contributions to R_a will be approximately equal, i.e., $R_a \sim \sqrt{ar}$. This is a very different conclusion than one which says that U_a must be chosen as high as possible. The lens equation [Eq. (1)] cannot be used for electrons which come from the end spoiling (group A electrons). Due to the fact that the end-spoiling region is almost field free, these electrons have a high probability to collide with the channel wall unless they come from the very end. The electrons emitted from the end of the end spoiling will gain a certain amount of kinetic energy in the radial direction (apart from the radial component of the emission energy) before the axial field significantly affects them. This is because the concentration of potential lines along the channel edge (plotted in Fig. 3) is relatively high and their orientation is almost parallel to the channel axis. Most of these electrons are able to escape to the anode gap. Reference 5 gives an analytical formula that describes the penetration of the electric field into an aperture along the optical axis (z). At the very end of the channel, this formula can be simplified to obtain

$$U(z, r=0) \approx \frac{E_a d}{2\pi}, \tag{5}$$

where d is the channel diameter. When it is assumed that the electrons from group A gain a certain fraction k of the potential in Eq. (5), as a radial energy component, one can write with Eq. (2):

$$(\text{group A})\ R_a = \left(\frac{2kad}{\pi}\right)^{1/2}, \tag{6}$$

where $0 \leqslant k \leqslant 1$. Note that Eq. (6) is independent of the anode voltage. Thus, R_a can be minimized by reducing the channel diameter and the anode gap. As an example, assume that $k = 1/2$. Then R_a becomes 40 μm (again, the default values are used). Note that this is twice as much as the radial displacement from the previous examples. Consequently, one would expect that group A electrons will contribute to a lower spatial resolution. This is in contradiction with the earlier mentioned statement from Koshida *et al.*

From this simple model, resulting in Eqs. (2), (4), and (6), it is clear that the influence on the spatial resolution of at least three parameters must be investigated: the anode voltage, the anode gap, and the channel diameter. Further, the influence of the end-spoiling penetration depth will be investigated because this parameter has a large influence on the energy distribution of the electrons that come out of the channels of a MCP.[2,3,6] The applicability of the very crude model used before will only become clear after comparison with the results of the full Monte-Carlo simulations.

To simulate the electron movement in the channel correctly, one has to define the distribution functions of the events. The model applies to a channel operated in conditions in which space charge and wall charging do not significantly modify the channel performance. It can easily be shown that in the operation range of all MCP image intensifiers these effects can be neglected.[7]

The usual assumption is to take the Poisson distribution for the statistical number of secondaries η generated by a primary electron hitting the channel surface. This distribution function is given by

$$f_1(\eta) = \frac{\delta^\eta}{\eta!}\exp(-\delta), \tag{7}$$

where $\delta(V, \gamma)$ is the secondary electron yield which can be calculated with the parameters V (the kinetic energy) and γ (the angle of incidence) of a given primary electron.[7,8] For a full simulation, one should then follow each secondary electron to its place of impact on the channel wall, create new secondary electrons, etc. However, because the number of electrons to be used is very large, we assume that this calculation procedure can be replaced by an exponential distribution of emitted electrons along the channel axis (z). This

stems from the fact that the process of multiplication in the channel is qualitatively the same for every z value. Thus, the gain G of the channel multiplier can be described by

$$G = C\langle \delta \rangle^p, \tag{8}$$

where C and p are constants (the latter for a given channel length). Consequently, the probability function for an electron to emerge from a certain z position at the channel wall becomes

$$f_2(z) = D \exp(q[z-l]), \quad f_3(\phi) = (2\pi)^{-1}, \tag{9}$$

where ϕ is the angle in the xy plane (i.e., the plane perpendicular to the z axis, or channel axis) and D and q are constants. The distribution is assumed to start at a depth l into the channel, and continues to the end spoiling depth. Of course, for the end-spoiling region a different distribution with other D and q values must be used.

Further, the start conditions of the secondary electrons have to be formulated.[7,8] The exit angles, θ and ϕ (spherical coordinate system), are described by a cosine distribution function

$$f_4(\theta) = \frac{\sin(2\theta)}{2}, \quad f_5(\phi) = (2\pi)^{-1}. \tag{10}$$

The kinetic energy V_0, at the moment the electron is emitted, is described by a Rayleigh distribution function[8]

$$f_6(V_0) = \frac{V_0}{\chi} \exp\left(\frac{-V_0^2}{2\chi}\right), \tag{11}$$

where χ is a constant.

In Fig. 4, the functions f_2, f_4, and f_6 are plotted, as obtained from a simulation with 15 000 electrons. The constants D, q, and χ are estimated by using experimental data from Refs. 8 and 9. It is assumed that the average secondary electron yield is 1.7 and the average length of the trajectories in the z direction is 30 μm (channel voltage=800 V; channel length=500 μm). The deeper into the channel the electrons are generated, the smaller the probability is that they leave the channel without hitting the channel wall. Therefore, the distribution does not have to start at the channel entrance, but can safely be started sufficiently deep (compared to the average trajectory length) into the channel, i.e., at $l=-200$ μm. This leads to $q=1.69\times10^4$ m^{-1} and $D=596$ m^{-1}. For the end spoiling, the average secondary electron yield is assumed to be unity (i.e., $q=0$) and the ratio of the end of the exponential distribution height and the constant end-spoiling distribution height is assumed to be 1.7, reflecting the ratio of secondary electron yields. A realistic energy distribution is obtained by choosing $\chi=2$, which sets the distribution maximum at $\sqrt{2}$ eV, in agreement with many published secondary electron energy distributions.

The electric field is calculated using the ELD program. Note that now also the lens field at the channel side of the end spoiling, which was neglected in the simple model, is taken into account. The main output file of ELD contains the potential on every mesh node in the design. This file (and a file containing the electron parameters) is used by the ray tracing program TRC/TRASYS[10] to calculate the trajectories of the particles. The integration routine, which solves the equations of motion, needs the field values along the path of the particle. The routine calculates the field from the 12 nearest mesh node potentials.[11]

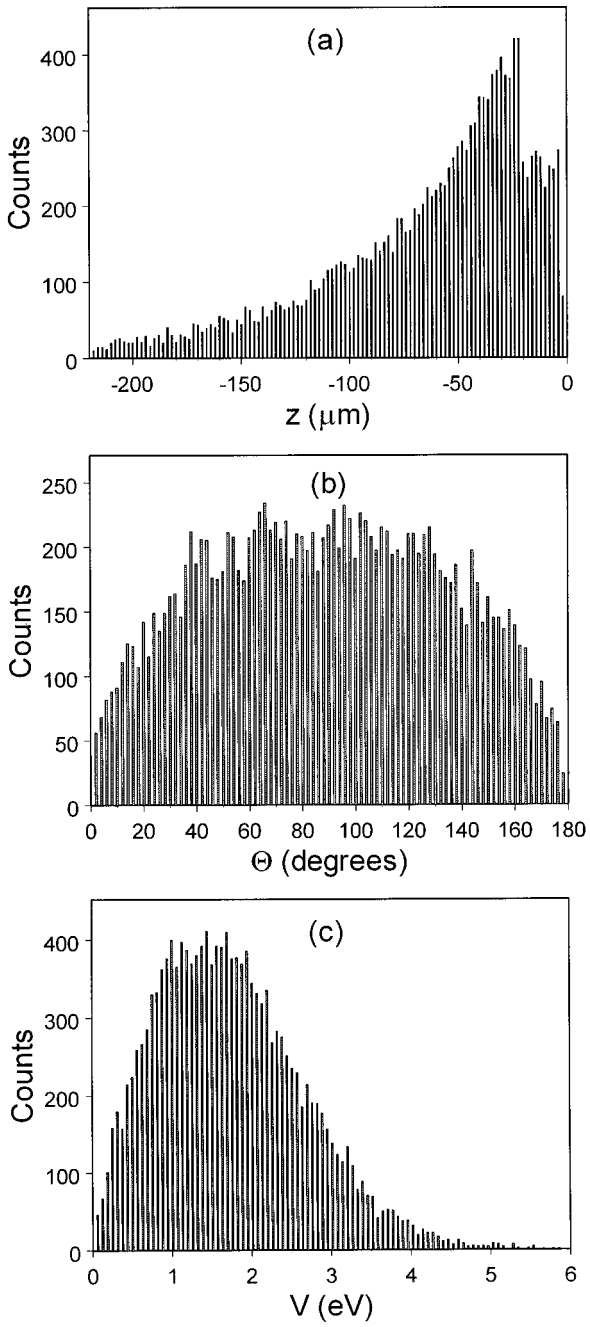

FIG. 4. (a) The exponential z distribution according to Eq. (9). The length of the linear interval is equal to the end-spoiling penetration depth. (b) The cosine θ distribution according to Eq. (10), and (c) the Rayleigh energy-distribution according to Eq. (11). To generate these plots, 15 000 electrons were used.

The simulations are fully three-dimensional. Every simulation is executed for 20 000 electrons. The spot on the anode always appeared to be almost rotationally symmetrical. This is an indication that the number of electrons is sufficiently

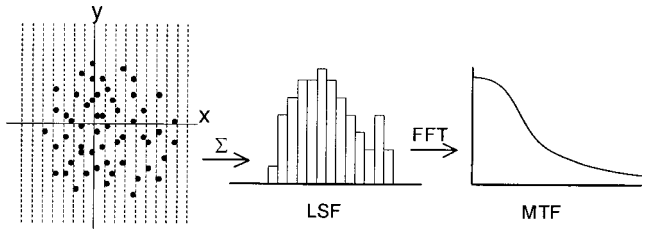

FIG. 5. This picture sketches how the MTF is obtained. From the current (electron) distribution in the spot (left) the LSF (middle) is obtained by summing (Σ) all electrons in each bar, and the MTF (right) is obtained by a FFT of the LSF.

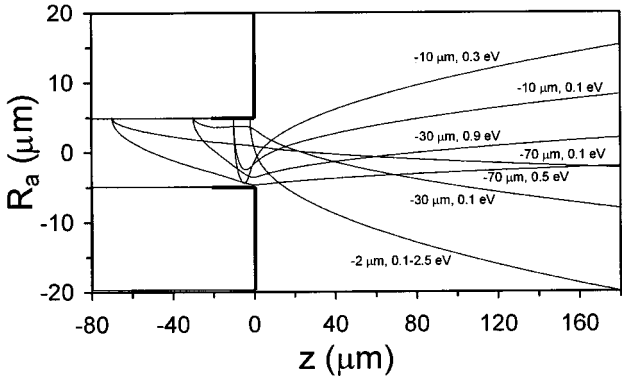

FIG. 6. Electron trajectories for the default configuration values. Electrons of two different energies are emitted from various depths: the end of the end spoiling ($z=-2$ μm), $z=-10$ μm, $z=-30$ μm, and electrons from deep down the channel ($z=-70$ μm).

large. Further, the results are reproducible within 1% for different seeds of the random generator.

The function chosen to represent the spatial resolution is the modulation transfer function (MTF). It is defined as the ratio of the image modulation to the object modulation and varies with the spatial frequency. The MTF is equal to the real part of the Fourier transform of the line spread function (LSF). It is convenient to take an equidistant line pattern as a measure for the spatial frequency. Then a certain spatial frequency is represented by a certain number of line pairs (lp) per millimeter. The MTF is often used to characterize the performance of optical systems as the MTF contains almost all optical information of a system, and it has the advantage that if the MTFs for the individual components in a system are known, the system MTF can simply be calculated as their product. Thus, by applying a relatively simple multiplication rule, the MTF of a complex system can be calculated from those of its components. The justification of these statements can be found in some advanced works on optical transfer functions, like Refs. 12 and 13.

The current distribution in the electron spot on the anode transforms into the corresponding LSF curve by dividing it into bars of equal width. In Fig. 5, a schematic spot profile on the anode is shown. The electrons in every bar are added to obtain the LSF and the MTF is obtained by a fast Fourier transform (FFT) of the LSF. The results of the simulations and experiments will be summarized in terms of the MTF at 25 and 60 line pairs per mm. These values are chosen as parameters to characterize the performance for the middle and high spatial frequencies, respectively. Both regimes are important when the image quality of a tube is concerned.[12]

III. SIMULATION RESULTS

To give a qualitative overview, the effect of the lens on the trajectories of electrons with different positions of emergence in the channel is displayed in Fig. 6. Note that this is a two-dimensional situation (i.e., emission perpendicular to the channel wall). Several representative values (from 0.1 to 2.5 eV) are used for the emission energy. In the earlier defined coordinate system from Fig. 2, the positions of emergence of the electrons are -2 and -10 μm (group A) and -30 and -70 μm (group B). For every z value, the trajectories of the 0.1 eV electron and the highest energy electron (i.e., the highest energy for which the electron is still able to get out of the channel) are shown. The parabolic shape of the trajectories in the channel, as well as in the anode gap, is clearly seen. Only the low-energy rays coming from just before the end spoiling (see the 0.1 eV ray starting at -30 μm in Fig. 6) are affected by the weak lens at the channel side of the end spoiling. The higher energy rays, as well as the rays from deeper down the channel, are already hardly affected by this lens, justifying the assumption of the simple model that this lens can be neglected compared to the lens at the anode side of the end spoiling. The focusing action of the latter lens is evident from the electron rays coming from before the end spoiling (region B). The electrons starting at -70 μm gain more axial energy (V_z) before crossing the lens, than the ones starting at -30 μm, and according to Eq. (4) their radial momentum change due to the lens will be smaller. Therefore, electrons coming from deeper down the channel end up closer to the center of the anode spot. Note that the anode is not visible in Fig. 6, as it is located at 500 μm. However, electrons generated in the end spoiling gain a lot of radial energy from the penetrating electric field, and their trajectories cross the anode plane much further from the spot center. Especially the electrons emerging from the very end of the end spoiling obtain a large radial energy and enlarge the spot size most. Note that in the -2 μm case all trajectories are almost the same, as the radial energy is predominantly determined by the electric field rather than the emission energy.

The quantitative results are obtained from the full simulations of 20 000 electrons. Figure 7 shows a typical MTF for the default configuration. Also indicated are the 25 and 60 lp/mm points, which will be used to compare the simulation results for different parameters. In Tables I and II the results are displayed for 25 and 60 lp/mm, respectively, and for varying anode gap and anode voltage. All other parameters are default values. Table I shows that the smallest gap and lowest voltage (300 μm, 3 kV) give the best result for 25 lp/mm. Larger gaps and/or larger voltages show a decrease of the MTF. From Table II (for 60 lp/mm) it is seen that for the larger gaps (500 and 800 μm), the optimum value of the voltage is near 5 kV. However, again the combination of a

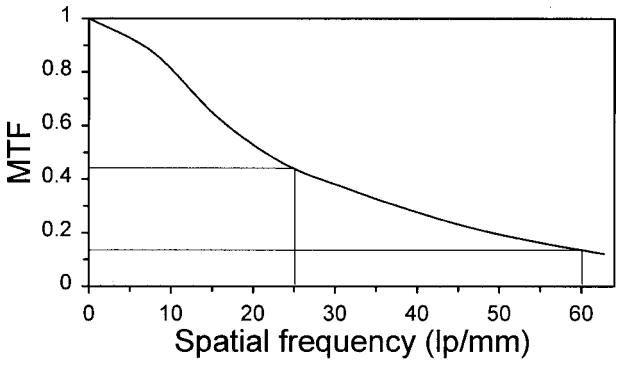

FIG. 7. Simulated MTF for the default configuration. The values at 25 and 60 lp/mm are indicated.

small gap and a low anode voltage is superior. The influence of the gap on the MTF is somewhat stronger than the influence of the anode voltage.

The two other parameters examined are the penetration depth of the end spoiling and the channel diameter. The results can be found in Tables III and IV, respectively. The end-spoiling penetration depth seems to be only important for the high spatial frequencies: from 10 to 20 μm, the MTF doubles for 60 lp/mm but the next step (20–30 μm) has no influence anymore. Further, it is very clear from Table IV that the channel diameter must be as small as possible, this parameter has an enormous influence on the MTF, for both 25 and 60 lp/mm.

IV. EXPERIMENTAL SETUP

To check whether the results from the simulations are realistic, comparative measurements were performed. The experimental setup is shown schematically in Fig. 8. The photocathode is replaced by a thermionic electron gun and the object is a microslit. (The channel plate consists of a large number of electron multiplier tubes in a hexagonal array. The image of a sharp slit through such an array of apertures depends on the relative position of the slit with respect to the array. If the slit is very long and not aligned with a principal axis of the array, the output image, averaged in time becomes independent of the position of the slit with respect to the array.) The spatial resolution can be checked with or without the MCP. The microscope reads the optical signal on the fiber output of the anode. Further, it magnifies the image because the resolution of the charge coupled device (CCD) camera (pixels of 9.12 μm) is too low for direct imaging. A very important feature of the design is the possibility of *in situ* variation of the anode gap. Changing this parameter, as well as the anode voltage, allows a full comparison between the simulations and the measurements.

TABLE I. Simulated MTF at 25 lp/mm for a variable anode voltage and anode gap.

	Anode gap (μm)		
Anode voltage (kV)	300 MTF	500 MTF	800 MTF
3	0.60	0.55	0.42
5	0.53	0.46	0.45
8	0.42	0.37	0.37

TABLE II. Simulated MTF at 60 lp/mm for a variable anode voltage and anode gap.

	Anode gap (μm)		
Anode voltage (kV)	300 MTF	500 MTF	800 MTF
3	0.26	0.08	0.02
5	0.16	0.12	0.04
8	0.04	0.06	0.03

Two examples of CCD-camera images can be found in Fig. 9. The top image [Fig. 9(a)] is a measurement with the MCP mounted; the bottom image [Fig. 9(b)] is the result for the anode, fiber optics and the measuring system (i.e., a measurement without the MCP). As is visible clearly, the MCP and anode gap have a large influence on the spatial resolution. The measurement without the MCP is done in order to correct for the influence of the phosphor grains, the fiber optics and the measurement system itself on the MTF because only the MCP and anode gap are under investigation. Further, the influence of the electron energy on the anode MTF appeared to be negligible.

V. EXPERIMENTAL RESULTS

The results of the measurements are shown in Tables V and VI. Due to limitations on the power supply, the anode voltage could only be raised to 7 kV. Experimentally it was difficult to adjust the anode gap exactly to the values for which the simulations were done. To enable an easy comparison between simulation and experiment, the experimental data were linearly interpolated to anode gap values as used in the simulations (for example, the result for 300 μm is calculated from the results for 250 and 360 μm). The small gaps and low voltages give the best results, as for the simulations. For 25 lp/mm, increasing the voltage (for 300 and 500 μm) or the anode gap (for 3 kV) results in a lower MTF.

The MTF, shown in Table VI (60 lp/mm), does not vary as strongly as in the simulations, but the trends are the same. Note that for 800 μm the MTF increases monotonically with the voltage because the proximity focusing effect of the anode gap field has become dominant over the defocusing lens effect at these relatively low anode gap fields.

TABLE III. Simulated MTF at 25 and 60 lp/mm and varying end-spoiling penetration depth *h*.

h (μm)	MTF at 25 lp/mm	MTF at 60 lp/mm
10	0.47	0.06
20	0.46	0.12
30	0.45	0.13

TABLE IV. Simulated MTF at 25 and 60 lp/mm and varying channel diameter *d*.

d (μm)	MTF at 25 lp/mm	MTF at 60 lp/mm
6	0.61	0.26
10	0.46	0.12
16	0.36	0.01

Finally, note that the earlier mentioned results are obtained with new MCPs. Even in this case, the MCP-to-MCP variation is considerable. Further, dirty MCPs (i.e., MCPs that are exposed to air for a longer period thus containing one or more layers of oxygen on the channel wall) show a worse MTF, while scrubbed MCPs (i.e., MCPs that are cleaned by an electron bombardment for typically 24 h) show a better MTF. A possible explanation of these observations lies in a change of the secondary electron yield. The oxides, attached on the dirty channel wall, have a high secondary electron yield. This could be equivalent to a steeper exponential distribution along the *z* axis (for the same gain). Consequently, the average energy of the output electrons becomes lower, which would influence the spatial resolution negatively.

VI. DISCUSSION AND CONCLUSIONS

When the results from the simulations (Tables I and II) and the measurements (Tables V and VI) are compared, it is clear that the global trends are the same. The combination 3 kV and 300 μm shows the largest MTF, both for 25 and 60 lp/mm. Increasing the anode voltage for a small anode gap leads to a smaller MTF, as well as increasing the anode gap at low anode voltages. For larger gaps the optimum voltage is near 5 kV.

How does the simple model [Eqs. (1)–(6)] explain the results? The most important observation from the results is the decrease of the MTF for a larger anode voltage and 300 μm gap, both for simulation and experiment. In this case, the contribution from Eq. (2) is small because *a* is small. Apparently, the lens [from Eq. (4)] indeed plays a crucial role in relation with the axial energy of the outcoming electrons, as it is also shown in Fig. 6. Note that the lens specifically affects the high spatial frequencies. This is because, when the anode voltage is increased sufficiently, the high energy electrons, which account for the large MTF at 60 lp/mm, will also be ''thrown away'' from the optical axis. There is a negative relation between MTF and anode gap, i.e., the MTF

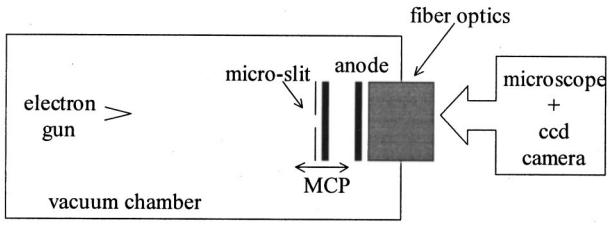

FIG. 8. Schematic drawing of the resolution measurement setup.

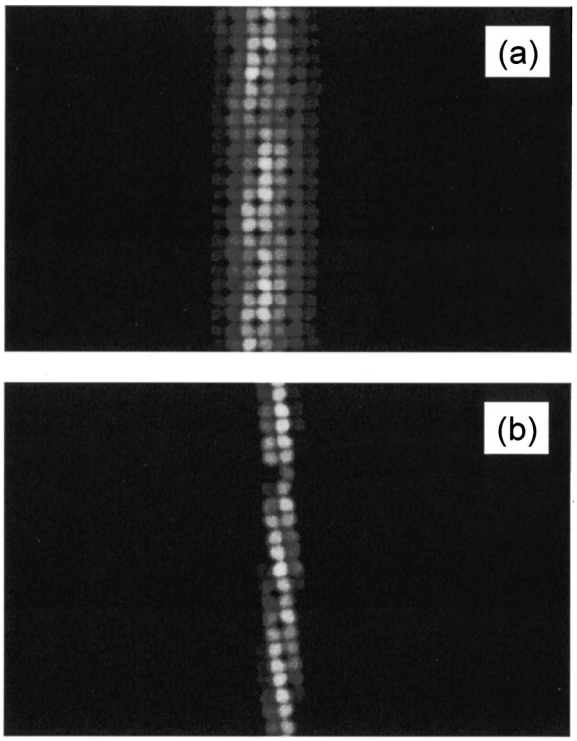

FIG. 9. Examples of the CCD image resulting from a measurement with (a) and without (b) a MCP. The ''pixel''-like image is caused by the fiber optics used. The fibers have a diameter of 4 μm.

TABLE V. Experimental MTF at 25 lp/mm for a variable anode voltage and anode gap.

	Anode gap (μm)		
Anode voltage (kV)	300 MTF	500 MTF	800 MTF
3	0.47	0.42	0.29
5	0.39	0.38	0.34
7	0.33	0.33	0.33

TABLE VI. Experimental MTF at 60 lp/mm for a variable anode voltage and anode gap.

	Anode gap (μm)		
Anode voltage (kV)	300 MTF	500 MTF	800 MTF
3	0.18	0.13	0.05
5	0.14	0.12	0.08
7	0.09	0.10	0.09

decreases for larger gaps. For small gaps, the anode voltage is of less importance but in most cases an optimum exists, as expected from Eqs. (2) and (4). For larger gaps, it is clear that the earlier mentioned proximity focusing effect comes in. This is the reason why the combination of 5 kV and 500 μm is used nowadays. Several technical problems arise when the combination of 3 kV and 300 μm has to be implemented in image tubes.

The simulations have shown that the influence of the channel diameter on the resolution is large, as illustrated by Table IV. The penetration of the electric field is approximately linear with the channel diameter, as shown by Eq. (5). Applying a smaller channel diameter will strongly increase the MTF of the system, mainly because the consequence of this measure is a smaller effect of the lens. This is consistent with Eq. (6). These findings were not verified experimentally. It is noteworthy that the simulation results can, surprisingly well, be understood from the simple model.

Finally, varying the end-spoiling penetration depth only modifies the MTF at 60 lp/mm. In case of a large end spoiling, most ''middle energy'' electrons, emitted from region B (i.e., the part of the channel before the end spoiling) will collide with the end-spoiling wall (because this region is almost field free). Thus, when the end-spoiling length is increased, the middle energy electrons will be caught by it. This is positive because the fraction of high energy electrons will increase. Obviously, only the first 20 μm of the end-spoiling accounts for this effect (see Table III). Electrons that are emitted from the end spoiling (especially from the end of it) are undesirable. These electrons have a high probability to escape into the anode gap. The electric field from the anode gap, which penetrates into the channel, will increase the radial energy of the electrons, and they will hit the anode far from the optical axis.

In conclusion it can be said that the spot size of electrons on the anode is largely determined by the lens. It has a defocusing effect on the spot size which, especially for the smaller gaps, dominates over the proximity focusing effect of a high, uniform electric field in the anode gap. The earlier mentioned authors[2,3] did not include the lens effect in their models. Further, they assumed that a monochromatic beam of *low* energy electrons would be preferable to achieve a higher MTF. However, the low energy electrons (mainly the electrons emitted from the end spoiling) appear to have a negative influence on the MTF. In order to raise the MTF of an image intensifier, the electrons from the end spoiling have to be excluded and/or the nonuniformity of the electric field near the end spoiling has to be suppressed.

[1]C. B. Johnson, S. B. Patton, and E. Bender, Inst. Phys. Conf. Ser. **121**, 193 (1992).
[2]N. Koshida, M. Midorikawa, and Y. Kiuchi, Adv. Electron. Electron Phys. **64b**, 337 (1985).
[3]N. Koshida and Y. Kiuchi, Adv. Electron. Electron Phys. **74**, 79 (1988).
[4]B. Lencová and G. Wisselink, Electrostatic Lens Design Program Package, licensed by Delft Particle Optics Foundation (1992).
[5]V. K. Zworykin, G. A. Morton, E. G. Ramberg, J. Hillier, and A. W. Vance, *Electron Optics and the Electron Microscope* (Wiley, New York, 1961).
[6]I. M. Bronshteyn, A. V. Yevdokimov, V. M. Stozharov, and A. M. Tyutikov, Radio Eng. Electron. Phys. **24**, 150 (1979).
[7]A. J. Guest, Acta Electron. **14**, 79 (1971).
[8]V. V. Apanasovich and E. G. Novikov, IEEE Trans. Electron Devices **42**, 2231 (1995).
[9]E. H. Eberhardt, Technical Note 127, ITT Electro-Optical Products Division, Fort Wayne, IN 46803 (1980).
[10]G. Wisselink, TRC/TRASYS Ray Tracing Package, licensed by Delft Particle Optics Foundation (1996).
[11]J. Chmelík and J. E. Barth, Proc. SPIE **2014**, 133 (1993).
[12]C. S. Williams and D. A. Becklund, *Introduction to the Optical Transfer Function* (Wiley, New York, 1989).
[13]E. Hecht, *Optics*, 3rd ed. (Addison Wesley, Reading, MA, 1988).